

# Transition to anomalous dynamics in a simple random map

Jin Yan\*

*Max Planck Institute for the Physics of Complex Systems, Nöthnitzer Str. 38, 01187 Dresden, Germany*

Moitrish Majumdar

*Department of Applied Mathematics, University of California, Merced,  
5200 N. Lake Road, 95343 Merced, California, United States of America*

Stefano Ruffo

*SISSA, Via Bonomea 265, 34136 Trieste, Italy  
INFN Sezione di Trieste, via Valerio, 2 34127 Trieste, Italy and  
Istituto dei Sistemi Complessi, via Madonna del Piano 10 - 50019 Sesto Fiorentino, Italy*

Yuzuru Sato

*RIES/Department of Mathematics, Hokkaido University,  
N12 W7 Kita-ku, Sapporo, 0600812 Hokkaido, Japan and  
London Mathematical Laboratory, 8 Margravine Gardens, London W6 8RH, United Kingdom*

Christian Beck

*School of Mathematical Sciences, Queen Mary University of London,  
Mile End Road, London E1 4NS, United Kingdom and  
The Alan Turing Institute, 96 Euston Road, London NW1 2DB, United Kingdom*

Rainer Klages

*School of Mathematical Sciences, Queen Mary University of London,  
Mile End Road, London E1 4NS, United Kingdom and  
London Mathematical Laboratory, 8 Margravine Gardens, London W6 8RH, United Kingdom  
(Dated: August 21, 2023)*

The famous Bernoulli shift (or dyadic transformation) is perhaps the simplest deterministic dynamical system exhibiting chaotic dynamics. It is a piecewise linear time-discrete map on the unit interval with a uniform slope larger than one, hence expanding, with a positive Lyapunov exponent and a uniform invariant density. If the slope is less than one the map becomes contracting, the Lyapunov exponent is negative, and the density trivially collapses onto a fixed point. Sampling from these two different types of maps at each time step by randomly selecting the expanding one with probability  $p$ , and the contracting one with probability  $1 - p$ , gives a prototype of a random dynamical system. Here we calculate the invariant density of this simple random map, as well as its position autocorrelation function, analytically and numerically under variation of  $p$ . We find that the map exhibits a non-trivial transition from fully chaotic to completely regular dynamics by generating a long-time anomalous dynamics at a critical sampling probability  $p_c$ , defined by a zero Lyapunov exponent. This anomalous dynamics is characterised by an infinite invariant density, weak ergodicity breaking and power law correlation decay.

A random dynamical system consists of a setting in which different types of dynamics are generated randomly in time. Here we consider a simple example, where an irregular or a regular dynamics is randomly selected at each discrete time step for determining the outcome at the next time step. By varying the sampling probability to select the one or the other dynamics, the completely irregular, respectively regular dynamics are recovered as limiting cases. Hence, there must be a transition between these two states. In our paper we explore this transition in detail. We find that there is a critical sampling probability at which the dynamics becomes anomalous by exhibiting a certain type of intermittency, i.e., a specific mixing between regular and irregular dynamics.

---

\* Email: jinyan@pks.mpg.de

## I. INTRODUCTION

Dynamical systems theory and the theory of stochastic processes generically refer to rather different fields of research. The former focuses on understanding the nonlinear and chaotic properties of typically deterministic dynamical systems, where the dynamics is completely determined by the initial conditions and the given equations of motion [1, 2]. Stochastic processes, in contrast, are governed by equations of motion containing random variables, which yields different outcomes when starting from the same initial conditions [3, 4]. Interestingly, deterministic dynamical systems may exhibit chaotic properties that, on a certain scale, can well be reproduced by a matching to stochastic processes [5, 6]. This is due to dynamical instabilities in the deterministic equations of motion leading to exponential separation of trajectories starting from nearby initial conditions [1, 2]. The resulting cross-link between deterministic and stochastic dynamics has been exploited particularly for understanding the emergence of irreversibility, transport and complexity on macroscopic scales in nonequilibrium statistical physics, starting from deterministic chaos in microscopic equations of motion [7–11]. This approach, which employs a suitable coarse-graining [12], amends a broad spectrum of conventional methods in nonequilibrium statistical physics, where stochastic randomness is put in by hand on a more microscopic level already [13, 14].

Another combination of deterministic and stochastic dynamics consists of what is called a random dynamical system [5, 15, 16]. According to Ref. [15], the origin of this field of research traces back to a short note by Ulam and von Neumann in 1945 about random ergodic theorems [17] that triggered a number of pioneering works. In random dynamical systems the equations of motion include random variables but are analysed within the framework of dynamical systems theory and ergodic theory. One might assume that all such systems can be understood by applying random perturbation theory [18] to the underlying deterministic dynamics. However, in general the randomness may not necessarily be small and could consist of any type of stochastic dynamics. Accordingly, it has been found that random dynamical systems may exhibit completely novel dynamical properties, such as random attractors [19–21] and their stochastic bifurcations [22, 23] as well as intricate statistical and ergodic properties [24–32] requiring a novel mathematical language for their description [33, 34]. This new theory has important applications to, e.g., fluid dynamics [20, 35], climate science [21, 36], and neural dynamics [37, 38].

More recently, it was shown that simple random dynamical systems can generate anomalous diffusion that matches to subdiffusive continuous time random walks [28], which continues a theoretical physics line of research starting from blow-out bifurcations and on-off intermittency [39–48]. Anomalous diffusion means that the mean square displacement (MSD) of an ensemble of particles increases nonlinearly in time,  $\langle x^2 \rangle \sim t^\alpha$  with  $\alpha \neq 1$ , while for normal diffusion  $\alpha = 1$ . This connects random dynamical systems theory with yet another big field of research, which is the theory of anomalous stochastic processes and their corresponding anomalous transport properties [49–53]. We remark that anomalous dynamics and anomalous transport are known to occur in deterministic dynamical systems [11, 50, 54–63] if they are weakly chaotic [11, 64–66], that is, there is still sensitivity to initial conditions, but the dynamical instability is weaker than exponential. In addition to this fully deterministic origin of anomalous dynamics, random dynamical systems thus provide a new access road to understand the emergence of anomalous dynamical properties at the interface between the theory of dynamical systems and stochastic theory [19, 28, 48].

A strikingly simple random dynamical system exhibiting anomalous dynamical properties was put forward in the paper by Pelikan Ref. [24]. Therein sufficient mathematical conditions were derived under which the invariant density of random maps is absolutely continuous. These theorems were illustrated by a specific example, a piecewise linear time-discrete random map on the unit interval that we call the Pelikan map, also studied in Refs. [31, 35, 67]; see Eqs. (2) given later and the respective discussion. This map displays a transition of the corresponding invariant density, under variation of a control parameter, from a uniform density, generated by chaotic dynamics with a positive Lyapunov exponent, to a density contracting onto a fixed point, associated with a negative Lyapunov exponent. For this map the absolutely continuous invariant density was calculated analytically in Ref. [24]. Inspired by this groundbreaking work and its cross-link to a simple diffusive model [68], in Ref. [28] a spatially extended map defined on the whole real line was introduced, where a suitably adapted version of the Pelikan map generated long-time diffusion. At a critical parameter value, determined by the Lyapunov exponent of this model being zero, the invariant density of the associated Pelikan-type map on the unit interval was computed numerically and found to be non-normalisable, known as an infinite invariant density [66, 69–71]. Consequently, the dynamics of the spatially extended system generated anomalous diffusion. Pelikan's paper is also related to an important body of rigorous mathematical works about random maps (see, e.g., Refs. [26, 31, 31, 32] and further references therein). Relevant for our setting are especially recent results by Homburg, Kalle et al.: Starting from random logistic maps exhibiting intermittency, synchronisation [27] and a respective transition in the invariant measure [72] they studied the decay of correlations in such systems [30] as well as invariant measures and associated Lyapunov exponents in piecewise linear random maps that are more general than the Pelikan map [73, 74].

Motivated by this framework, in the present paper we explore the non-trivial dynamical transition scenario of the original Pelikan map in more depth. In particular, we calculate a suitably coarse-grained functional form of the

invariant density, a simple ergodicity breaking parameter, and the position autocorrelation function under parameter variation by characterising this transition in terms of these three quantities. Exact and approximate analytical results are compared with computer simulations. Our results for the invariant density enable us to precisely identify the different dynamical regimes exhibited by this random map during the transition. By considering a mean current as an observable we obtain numerical evidence for ergodicity breaking at the transition point. Correspondingly, we find that the autocorrelation function displays a transition from exponential to power-law decay when approaching the critical parameter value. We thus arrive at a detailed characterisation of the whole transition scenario in this random map. This transition, being of on-off type as in a certain class of deterministic dynamical systems [28, 39–48, 75], turns out to be very different from the seemingly similar transition to intermittency in the paradigmatic Pomeau-Manneville map [76–80]. What we study here is probably one of the simplest non-trivial examples of a random dynamical system. The great advantage of this system is that many results can be proved analytically, demonstrating for a generic case how anomalous properties of random dynamical systems emerge from first principles. Many of the phenomena that we describe in this paper may arise in other, more complex systems as well, as long as there is a transition scenario where a parameter is changed that controls the relative likelihood of a contracting dynamics alternating with an expanding one [28].

We proceed as follows: In Sec. II we introduce our random dynamical system, the Pelikan map, and calculate its corresponding invariant density both analytically and numerically. We summarise our results in a table outlining the whole transition scenario. Furthermore, we provide numerical evidence for weak ergodicity breaking by studying a relevant observable. In Sec. III we calculate the position autocorrelation function of this random map analytically exactly, approximately, and by simulations, and compare the results with each other. Section IV concludes with a brief summary and an outlook. All detailed calculations are shifted to the Appendix.

## II. TRANSITION TO INTERMITTENCY IN THE PELIKAN MAP

### A. The Pelikan map

We consider one-dimensional maps

$$x_{n+1} = T(x_n), \quad (1)$$

where  $n \in \mathbb{N}$  is discrete time and  $x \in [0, 1)$  the position of a point on the unit interval. Our maps are piecewise linear with uniform slope  $s > 0$ . To construct a simple random dynamical system  $T(x)$ , we sample from two maps  $T_1(x), T_2(x)$  with different values of the slope  $\{s_1, s_2\}$  randomly in time. That is, at each time step  $n$  one of the two maps is chosen randomly with a probability  $p \in [0, 1]$ , respectively  $1 - p$ . In particular, we choose  $s_1 > 1$  and  $s_2 < 1$  so that  $T_1(x)$  is expanding with positive Lyapunov exponent  $\lambda_1 = \ln s_1 > 0$  and thus chaotic, while  $T_2(x)$  is contracting with negative Lyapunov exponent  $\lambda_2 = \ln s_2 < 0$ . More specifically, we consider the case of

$$T(x) = \begin{cases} T_1(x) = s_1 x \bmod 1 & \text{with probability } p \\ T_2(x) = s_2 x & \text{with probability } 1 - p. \end{cases} \quad (2)$$

For the parameter values  $s_1 = 2 = 1/s_2$  we call the random map  $T$  the *Pelikan map*, as, to our knowledge, it was first studied by Pelikan [24], later also in Refs. [35, 67]; see Refs. [26, 29, 74] for related examples. In the remainder of the paper, we mostly focus on the Pelikan map. The values of  $p = 0$  and  $p = 1$  define two deterministic limiting cases for which  $T$  is well understood: In the latter case  $T = T_1(x)$  reproduces the well-known Bernoulli shift as studied in many textbooks [1, 2, 5, 6]. The former case  $T = T_2(x)$  yields a simple contraction on the unit interval, where all points converge towards the stable fixed point at  $x = 0$ . However, for  $0 < p < 1$  stochastic randomness sets in generating a dynamical transition from global contraction at  $p = 0$  to uniform chaos at  $p = 1$ . To understand this transition under variation of  $p$  is the main topic of our paper.

### B. Invariant density

We first study the invariant density  $\rho_p(x)$  of the Pelikan map under variation of  $p$ , which characterises the equilibrium states of the random dynamics. For  $0 \leq p < 1/2$ ,  $\rho_p(x)$  is trivially the delta function at the stable fixed point  $x = 0$ , as the map  $T$  is on average contracting [1]. For  $1/2 < p \leq 1$  it has been proven in Ref. [24] that  $T$  exhibits a unique absolutely continuous invariant measure, whose support is all of  $[0, 1)$ , with an invariant density that is piecewise constant over the partition  $\{[2^{-(n+1)}, 2^{-n}]\}_{n \in \mathbb{N}_0}$  of the unit interval. This is shown in the first row of Fig. 1, which

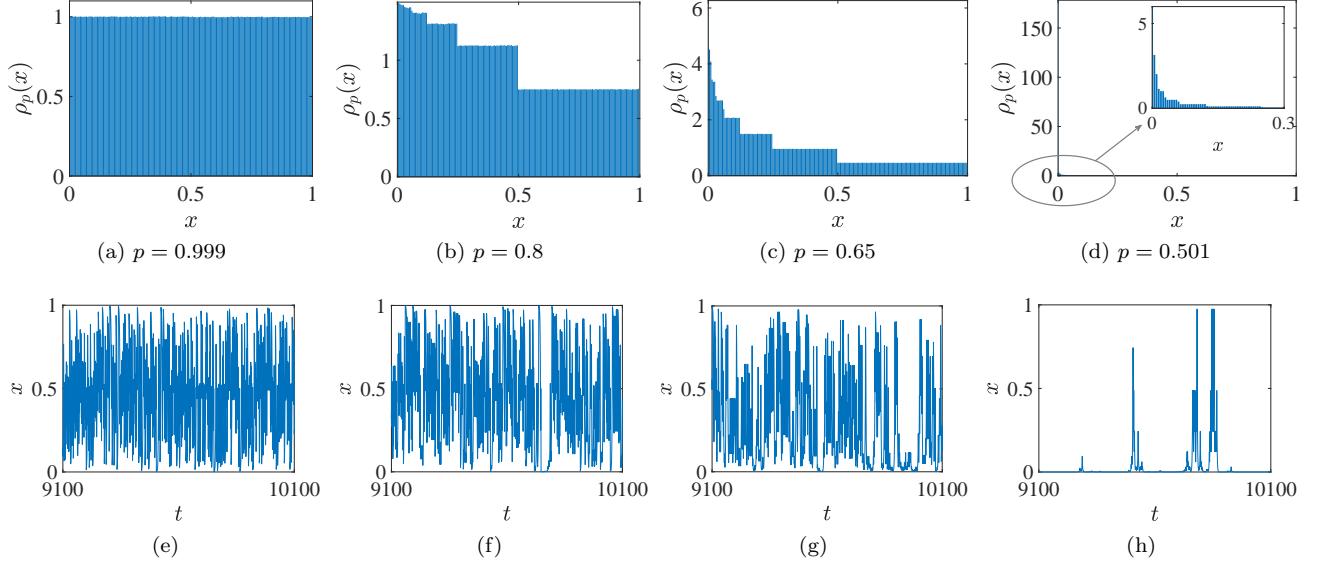


FIG. 1: Invariant density  $\rho_p(x)$  (upper row) for different values of the sampling probability  $p \in (0.5, 1)$  and corresponding typical trajectories (lower row) of the Pelikan map  $T$ , defined by Eq. (2) for particular values of the two slopes as explained in the text. The values of  $p$  are given below the upper row. Each histogram is generated from computer simulations by iterating  $10^4$  initial points (uniformly randomly chosen) for 10100 time steps, with the first 100 iterations discarded to eliminate transients. The bin size in each histogram is  $\Delta x = 1/200$ . One can see that the density becomes singular around  $x = 0$  for  $p \rightarrow 1/2$ , cf. the values along the  $y$  axis and the blow-up in the inset of (d). The time window for all trajectories in the lower row is  $t \in [9100, 10100]$ .

depicts  $\rho_p(x)$  obtained from computer simulations for representative values of  $p$ . In the second row of Fig. 1, we see that close to  $p = 1/2$  a typical trajectory exhibits intermittency [2, 5, 76, 77], that is, it displays irregular chaotic bursts within long regular motion close to the stable fixed point.

Along with the existence and uniqueness result for  $\rho_p(x)$ , in Ref. [24] an iterative formula has been derived for it yielding the value on each partition part where the density is piecewise constant. While this formula is exact, it does not elucidate the coarse grained, generic functional form of  $\rho_p(x)$  and how it changes under variation of  $p$ . As we will show below, calculating such an expression makes it easier to characterise the whole transition, and to compare  $\rho_p(x)$  with the invariant density of other intermittent chaotic dynamical systems, in particular the Pomeau-Manneville map [76, 77]. For this purpose, we determine a coarse-grained invariant density by joining the midpoints of all pieces where  $\rho_p(x) = \text{const.}$  (cf. the orange curve in Fig. 2a). Its functional form can be derived analytically from the normalisation condition for  $\rho_p(x)$ ,  $p \in (1/2, 1]$ . By using the amplitudes  $a_i := \rho_p|_{(2^{-(i+1)}, 2^{-i})}$  and the areas under constant pieces of the invariant density  $\rho_p$ ,  $r_i := \int_{2^{-(i+1)}}^{2^{-i}} \rho_p dx$ ,  $i \in \mathbb{N}_0$ , cf. Fig. 2a, the normalisation reads  $\sum_{i=0}^{\infty} r_i = 1$ . Furthermore,  $a_i$  and  $r_i$  satisfy  $a_n = 2^{n+1}r_n$  and the following recursion relations [24],

$$\frac{r_{n+1}}{r_n} = \frac{-1 + \left(\frac{2(1-p)}{p}\right)^{n+2}}{-2 + 2\left(\frac{2(1-p)}{p}\right)^{n+1}}, \quad \frac{a_{n+1}}{a_n} = 2\frac{r_{n+1}}{r_n}, \quad n \in \mathbb{N}_0. \quad (3)$$

This gives for the first amplitude  $a_0 = (2p - 1)/p$ , and recursively we have (see App. A)

$$a_n = \frac{-1 + \left(\frac{2(1-p)}{p}\right)^{n+1}}{-1 + \frac{2(1-p)}{p}} a_0 = \frac{2p-1}{3p-2} \left[ 1 - \left(\frac{2(1-p)}{p}\right)^{n+1} \right]. \quad (4)$$

To distinguish the exact discontinuous invariant density  $\rho_p$  from its coarse-grained functional form, we denote the latter by  $\tilde{\rho}_p$ . This is in turn given by taking the limit  $n \rightarrow \infty$  of the mid-points  $(3/2^{n+2}, a_n)$  leading to (see again App. A),

$$\tilde{\rho}_p(x) = A(1 - Bx^{-1+C}), \quad p \in \left(\frac{1}{2}, 1\right), p \neq \frac{2}{3}, \quad (5)$$

where

$$A(p) = \frac{2p-1}{3p-2}, \quad B(p) = \left( \frac{2(1-p)}{p} \right)^{\frac{\ln 3}{\ln 2} - 1}, \quad C(p) = \frac{1}{\ln 2} \ln \frac{p}{1-p}. \quad (6)$$

The invariant density curves  $\tilde{\rho}_p$  for various values of  $p \in (0.5, 1)$  are plotted in Fig. 2b. For  $p \rightarrow 1^-$  we see that  $\tilde{\rho}_p \rightarrow 1$ , which is the result for the deterministic Bernoulli shift [1, 2, 5, 6]. However, as  $p \rightarrow 1/2^+$  we have  $C(p) \rightarrow 0$ , consequently  $\tilde{\rho}_p(x)$  behaves as  $1/x$  (normalisation is governed by the factor  $A$ ). In particular, at  $p = 4/5$  we have  $A = 3/2$ ,  $B = 2/3$ ,  $C = 2$  and the curve becomes linear,  $\tilde{\rho}_{p=0.8}(x) = 3/2 - x$ . Consequently, as the parameter  $p$  decreases from 1 to 0, the random map  $T$  undergoes a rather non-trivial dynamical transition: At  $p = 1$  we have a uniform density  $\tilde{\rho}_p$  representing fully chaotic dynamics. For  $1 > p$  this density becomes non-uniform by decreasing monotonically. At  $p = 4/5$  the curvature of the density changes from concave to convex. At  $p = 2/3$  the density develops a singularity at  $x = 0$ , which remains normalisable for  $2/3 > p > 1/2$  (see Ref. [26] for related results regarding a randomised tent map), hence the system exhibits stationary intermittency. At  $p = 1/2$  there is a transition to non-stationary intermittency, where the system possesses both an unbounded but normalisable (in that sense ‘physical’) invariant density  $\delta(0)$  and an unbounded, non-normalisable (infinite) invariant density  $\tilde{\rho}_p$  (see Ref. [31] for a rigorous mathematical analysis of this case). Finally, for  $1/2 > p \geq 0$  global contraction leads to a density that collapses onto the singular but normalisable delta function at the fixed point  $x = 0$ . A similar transition scenario has been described for a related but more complicated random map in Ref. [29].

This rich scenario represented by  $\tilde{\rho}_p$  under variation of  $p$  may be compared with the transition to intermittency exhibited by the Pomeau-Manneville map,  $P(x) = x + sx^z \mod 1$ ,  $s \geq 1$ ,  $z \geq 1$ , by varying  $z$  for fixed  $s$  [76–80]. At first view there are some striking similarities: In analogy to the Pelikan map  $T$ , for  $s = 1$  and  $z = 1$  this map  $P$  reduces to the Bernoulli shift. And similar to the density of  $T$  for  $p \rightarrow 1/2$ , for  $z \rightarrow 2$  the density of  $P$  becomes non-integrable. At the transition points both maps develop infinite invariant densities [66, 69] with even the same singularity, i.e.,  $\rho_{PM}(x) \sim 1/x$  for  $P$  at  $z = 2$  [81] and  $\tilde{\rho}_p \sim 1/x$  for  $T$  at  $p = 1/2$  [28, 40, 42, 44, 46–48, 67]. However, in further detail these two transition scenarios are completely different:  $P$  remains deterministic for all  $z$  and is characterised by a smooth invariant density  $\rho_{PM}(x) \sim x^{1-z}$  for all  $z > 1$  [81–86] while  $T$  is random for all  $0 < p < 1$ , and its exact invariant density  $\rho_p$  is piecewise constant, see Eqs. (3),(4). Furthermore, in sharp contrast to the coarse-grained density  $\tilde{\rho}_p$  of  $T$ , see Eqs. (5),(6) and as discussed above, the transition scenario of  $P$  is much simpler: Its density immediately becomes singular for all  $z > 1$  and is still integrable for  $1 < z < 2$  but as a convex power law. It is indeed known [28, 35, 67] that the transition exhibited by  $T$  belongs to the class of on-off intermittency [39–48, 75], which is different to the one of  $P$ . We remark that the Pelikan map appears to be one of the very few examples of a random dynamical system for which the invariant density can be calculated exactly analytically for all parameter values.

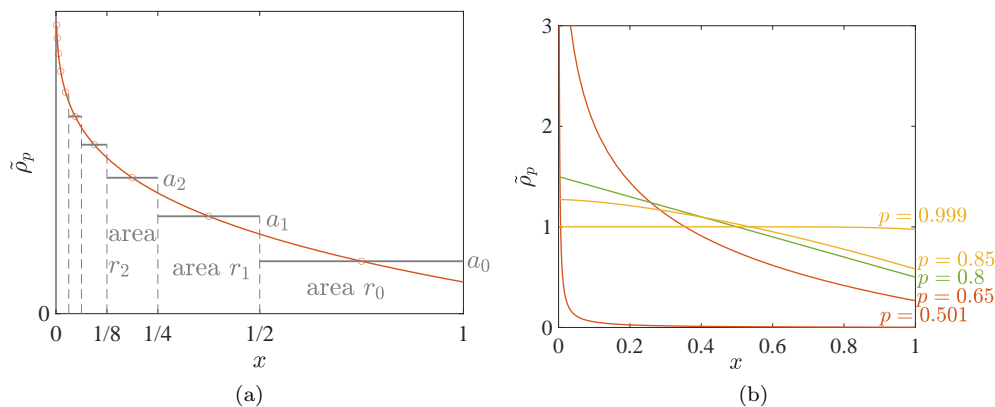


FIG. 2: (a) Construction of the coarse-grained invariant density  $\tilde{\rho}_p(x)$  (in orange, curved line) for the Pelikan map  $T$  with  $p \in (0.5, 1)$ . The original exact invariant density  $\rho_p(x)$  is given by the piecewise constant amplitudes  $a_i$  (in black) and the associated areas  $r_i$ ,  $i \in \mathbb{N}_0$ , cf. Fig. 1. The corresponding  $\tilde{\rho}_p$  is defined by the mid-points of all amplitudes. (b) Invariant density  $\tilde{\rho}_p(x)$ , plotted by using Eqs. (5),(6), for  $p = 0.999, 0.85, 0.8, 0.65$  and  $0.501$  (cf. Fig. 1). The change of colour indicates the change in convexity of the curves at  $p = 0.8$ , cf. also the  $p$  values to the right.

### C. Dynamical instability

We now discuss dynamical stability properties of the Pelikan map in terms of its Lyapunov exponent  $\lambda$  under variation of  $p$ . In order to do so, we first refine our notation for capturing particular realisations of a noise sequence. Let  $\omega_i$  be a random variable for which at any time step  $i \in \mathbb{N}$  one of two integer values  $\omega_i \in \{1, 2\}$  is chosen randomly with probability  $p$ , respectively  $1 - p$ . These two values determine correspondingly which of the two maps  $T_i(x)$ ,  $i = 1, 2$ , is applied at time step  $i$ , according to Eq. (2), for generating the position at the next time step  $i + 1$ , according to Eq. (1). Let  $\Omega_n = \{\omega_i\}_{i=1}^n$  denote the realisation of a particular noise sequence up to time  $n$ . With the symbol  $\Omega$  we label the dependence of an observable on the realisation of a particular noise sequence  $\Omega_n$  in the limit of  $n \rightarrow \infty$ . Based on these preliminaries, we define two different types of averages for the Pelikan map [87]

1. The time-averaged Lyapunov exponent [21, 28]

$$\lambda_t = \int \lambda_t(\Omega) \varrho(\Omega) d\Omega \quad (7)$$

with

$$\lambda_t(\Omega) = \lim_{n \rightarrow \infty} \frac{1}{n} \sum_{i=1}^n \ln |T'(x_i(\Omega_i))|, \quad (8)$$

where  $\varrho(\Omega)$  is the distribution of the noise. With  $x_i(\Omega_i)$  we denote the dependence of the position of a point at time step  $i$  on the particular realisation of the noise sequence  $\Omega_i$ . In the deterministic case, i.e.,  $p = 0$  or  $p = 1$ , this average boils down to

$$\lambda_t^d = \lim_{n \rightarrow \infty} \frac{1}{n} \sum_{i=1}^n \ln |T'(x_i)|. \quad (9)$$

2. The ensemble-averaged Lyapunov exponent

$$\lambda_e = \int \ln |T'(x(\Omega))| \rho_p(x(\Omega), \Omega) d\Omega dx, \quad (10)$$

where  $\rho_p(x) = \int \rho_p(x(\Omega), \Omega) d\Omega$  holds for the invariant density of the system, by assuming that it exists. In the deterministic case this average boils down to

$$\lambda_e^d = \int \ln |T'(x)| \rho_p(x) dx. \quad (11)$$

Let us now calculate both types of Lyapunov exponents for map  $T$ . Due to the uniform slope of  $T$ , the time-averaged Lyapunov exponent is obtained straightforwardly to [28]

$$\lambda_t = p \ln 2 + (1 - p) \ln \frac{1}{2} = (2p - 1) \ln 2. \quad (12)$$

It is thus well-defined for all  $p$ . In particular, it vanishes at  $p = 1/2$ , which coincides with the transition to non-normalisability of the invariant density [28]. For the ensemble-averaged Lyapunov exponent we observe that  $\text{Prob}[\ln |T'(x(\omega_i))| = \ln 2] = p$  and  $\text{Prob}[\ln |T'(x(\omega_i))| = \ln(1/2)] = 1 - p$  at any time step  $i$ , according to Eq. (2), and due again to the uniformity of the slope therein. Averaging over the (in this case dichotomic) noise in Eq. (10) then yields

$$\lambda_e = p \ln 2 + (1 - p) \ln \frac{1}{2} = (2p - 1) \ln 2, \quad p \neq \frac{1}{2}. \quad (13)$$

At  $p = 1/2$  we have the infinite density  $\rho_p$ , whose non-normalisability defies a unique result for  $\lambda_e$ . We conclude that time- and ensemble-averaged Lyapunov exponent for map  $T$  are equal,  $\lambda_t = \lambda_e$ , for  $p \neq 1/2$ . In this sense, we consider the system to be ergodic for  $p \neq 1/2$ , and clearly it is chaotic when  $1/2 < p \leq 1$ .

It should be noted that, in some random dynamical systems, the numerically observed Lyapunov exponent can be negative yet the system still exhibits chaotic behaviour [22, 88]. In such systems the Lyapunov exponent has no definite value and is described by a distribution with a non-zero tail in the positive regime, although the peak may lie

parameter	invariant density $\rho_p(x)$ , $x \in [0, 1]$	Lyapunov exponent	dynamics
$p = 1$	uniform density $\rho_1(x) = 1$	$\lambda_t^d = \lambda_e^d = \ln 2$	$T = T_1$ uniformly chaotic
$1 > p \geq \frac{2}{3}$	bounded and normalisable	$\lambda_t = \lambda_e = (2p - 1) \ln 2$	chaotic
$\frac{2}{3} > p > \frac{1}{2}$	unbounded but normalisable	$\lambda_t = \lambda_e = (2p - 1) \ln 2$	stationary intermittency
$p = \frac{1}{2}$	unbounded and non-normalisable	$\lambda_t = 0$ , $\lambda_e$ : undefined	non-stationary intermittency
$\frac{1}{2} < p < 0$	$\delta(0)$	$\lambda_t = \lambda_e = (2p - 1) \ln 2$	global contraction on average
$p = 0$	$\rho_0(x) = \delta(0)$	$\lambda_t^d = \lambda_e^d = -\ln 2$	$T = T_2$ global contraction

TABLE I: Summary of dynamical properties of the Pelikan map, characterised by the invariant density and the Lyapunov exponent.

in the negative regime. For more general random dynamical systems, Lyapunov exponents may not reveal dynamical properties such as topological bifurcations of attractors [22]. Along these lines, for the Pelikan map with  $0 < p < 1/2$  one can observe chaotic dynamics for finite time, in the sense of a chaotic transient, with a positive probability, but the Lyapunov exponent is negative. In contrast, the Pomeau-Manneville map is characterised by ergodicity and a positive Lyapunov exponent for  $1 \leq z \leq 2$ , while it exhibits a stretched exponential dynamical instability leading to a zero Lyapunov exponent, and infinite ergodicity, for  $z > 2$  [66, 78, 79]. In Table I we summarise the transition to intermittency in the Pelikan map.

We remark that one can generalise our above analysis to the case where  $s_1 = 1/s_2$  [89]. It turns out that for these specific slopes the random dynamical system Eq. (2) still possesses a regular partition with a piecewise constant invariant density. On this basis one can show that the normalisability still changes at  $p = 1/2$ , always coinciding with the vanishing of the time-averaged Lyapunov exponent given by  $\lambda_t = (2p - 1) \ln s_1$ , and the boundedness changes at  $p = s_1/(s_1 + 1)$ . The convexity change occurs at  $p = s_1^2/(s_1^2 + 1)$ , as is shown in App. B. We note that related, rigorous results have been obtained in Ref. [90]. Here, for  $s_1, 1/s_2 \geq 2$  it was proven that in the corresponding random map there exist different invariant measures under variation of  $p$  depending on the associated Lyapunov exponent, which supports our findings. A generalised version of the setting in Ref. [90] is studied in Ref. [74].

#### D. Ergodic properties

We finally study in some more detail the ergodic properties of the Pelikan map with respect to the non-trivial transition at  $p = 1/2$ . If we consider a new variable  $y_n$ , defined via the Birkhoff sum of iterates of the Pelikan map with the mean subtracted [91],

$$y_{n+1} = y_n + x_{n-1} - \langle x \rangle = \sum_{k=0}^{n-1} (x_k - \langle x \rangle), \quad (14)$$

the average of  $y_{n+1}$  can be determined by averages of  $x_k$  and  $x$  as

$$\langle y_{n+1} \rangle = \left\langle \sum_{k=0}^{n-1} (x_k - \langle x \rangle) \right\rangle = \left\langle \sum_{k=0}^{n-1} x_k \right\rangle - n \langle x \rangle. \quad (15)$$

Here we denote by  $\langle \dots \rangle$  the combined noise and ensemble average. In Fig. 3 we see from simulations that for all  $p > 1/2$  the averaged Birkhoff sum  $\langle \sum_{k=0}^{n-1} x_k \rangle$  increases linearly with time  $n$ , while for  $p \rightarrow 1/2^+$  it changes to sub-linearly. This nonlinear behaviour of  $\langle \sum_{k=0}^{n-1} x_k \rangle$  can be considered as an indicator of weak ergodicity breaking [92–94], in the sense that  $\langle y_{n+1} \rangle = n \left( \frac{1}{n} \langle \sum_{k=0}^{n-1} x_k \rangle - \langle x \rangle \right) \neq 0$  implies that the time average of  $x_k$  is not equal to the ensemble average for the Pelikan map.

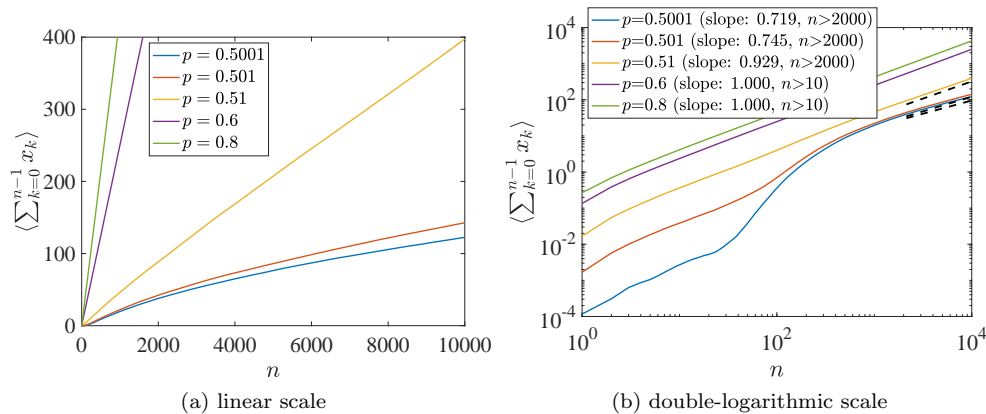


FIG. 3: The noise-ensemble average  $\langle \sum_{k=0}^{n-1} x_k \rangle$  as a function of time  $n$ , taken over  $10^4$  initial points (sampled directly from the invariant density formula with a truncation of 20 subintervals on  $[0, 1]$ ), and time up to  $n = 10^4$ . (a) shows results on a linear scale, (b) depicts a double-logarithmic plot. In (b), the dashed lines for  $p = 0.5001, 0.501$  and  $0.51$  are linear fits from time  $n > 2000$ . The slopes are given in the legend, in comparison to  $p = 0.6$  and  $0.8$  (linear fits from  $n > 10$ ), where the slopes are 1.

### III. POSITION AUTOCORRELATION FUNCTION

Correlation functions are important quantities characterising dynamical systems. Their decay in time is intimately related to fundamental ergodic properties like mixing [5, 6]. In the form of velocity autocorrelation functions they can be used to calculate transport coefficients of dynamical systems via (Taylor-)Green-Kubo formulas [10, 11, 62, 63]. For simple deterministic piecewise linear maps, including the Bernoulli shift, position autocorrelation functions have been calculated analytically in Ref. [95]; see also [96]. Here we focus on the position autocorrelation function of the Pelikan map, defined as the ensemble average of the product of two positions at different times,

$$\langle x_{k+t} x_t \rangle = \langle x_k x_0 \rangle = \int \rho_p(x_0) T^k(x_0) x_0 dx_0, \quad k, t \in \mathbb{N}. \quad (16)$$

Note that this ensemble average is defined with respect to the invariant density  $\rho_p$  of the map, according to which the initial conditions are distributed. This implies that we can simplify the first product to the second one by using stationarity, respectively time translational invariance. In the following we first compute this autocorrelation function numerically over the whole range of  $p \in (1/2, 1]$ , up to somewhat larger times. We then calculate it exactly analytically for the same range of  $p$  at the first three time steps. As calculating exact results for larger times becomes too tedious, we then develop an analytical approximation that gives some insight into the asymptotic decay particularly for  $p \rightarrow 1/2$  and  $p \rightarrow 1$ .

#### A. Simulation results

To compare results of the position autocorrelation function Eq. (16) for different values of  $p \in (1/2, 1]$ , we define the normalised correlation function (nCF)

$$\text{nCF}(p, k) := \frac{\langle x_k x_0 \rangle - \langle x \rangle^2}{\langle x_0^2 \rangle - \langle x_0 \rangle^2}, \quad (17)$$

which we have computed numerically. There are two main subtleties for the numerical simulations. First, by definition the Pelikan map involves a binary shift operation (and its contraction counterpart). But since any computer stores numbers in finite 0-1 bits, high-precision simulations are needed to accurately obtain autocorrelations for large times, otherwise the computer memory would run out of bits, and nothing can be shifted anymore. For our simulations we have thus used a high-precision algorithm from the GNU MPFR library in C [97]. Second, as  $p$  approaches the critical value of  $1/2$ , where the invariant density becomes non-normalisable, preparing such a highly singular initial distribution becomes increasingly difficult. Instead of obtaining initial conditions directly from the density formula, one could start from an arbitrary distribution and wait until it approximately reaches an equilibrium. However, for



$p \rightarrow 1/2$  the transient time becomes extremely long. We have tested both methods but eventually decided to use the former. Figure 4 presents simulation results for Eq. (17). In Fig. 4(a) we see that, as expected, there is clean exponential decay for  $p = 1$ . That there is exponential decay of correlations for  $p > 1/2$  in the limit of large enough times was already proven in Refs. [24, 26], and our numerical findings are in line with this result. Interestingly, Fig. 4(b) shows a transition to a clean power law decay for  $p \rightarrow 1/2$ . In the following we will compare these numerical results with exact and approximate analytical results by confirming our findings.

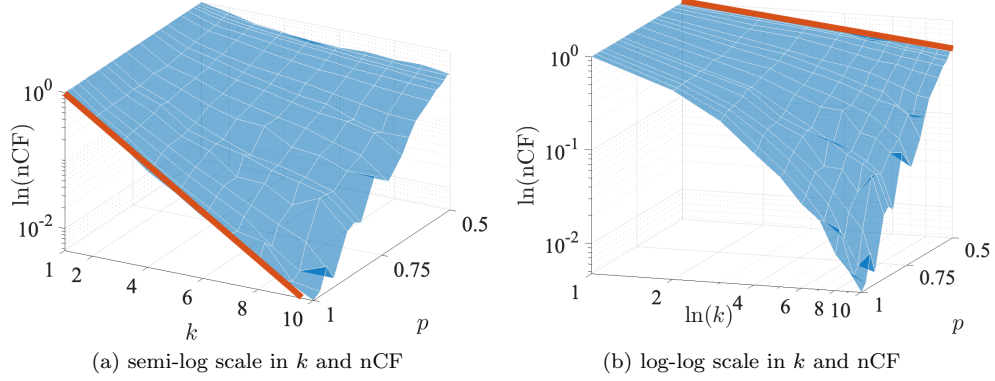


FIG. 4: Simulation results for the normalised position autocorrelation function nCF Eq. (17) as a function of both  $p \in (0.5, 1)$  and time  $k = 1, \dots, 9$ . The graphs are generated by averaging over  $10^5$  initial points sampled directly from the invariant density formula (with a truncation of 20 subintervals of the unit interval). 25 values of  $p$  have been used between 0.5001 and 0.9999, with more values closer to 0.5.

### B. Exact analytical results for small times

We now present exact analytical results for the autocorrelation decay at the first three time steps. For  $k = 1$ , the first term of the correlation function Eq. (16) can be calculated to

$$\begin{aligned} \langle x_1 x_0 \rangle &= p \int_0^1 \rho_p(x_0) T_1(x_0) x_0 dx_0 + (1-p) \int_0^1 \rho_p(x_0) T_2(x_0) x_0 dx_0 \\ &= 2p \langle x^2 \rangle - a_0 p \int_{\frac{1}{2}}^1 x dx + \frac{1-p}{2} \langle x^2 \rangle \\ &= \frac{(2p-1)(3p+25)}{24(5p-1)}, \end{aligned}$$

where we have used the second moment  $\langle x^2 \rangle = \int \rho_p(x) x^2 dx = \frac{4(2p-1)}{3(5p-1)}$  (App. C). Deriving correlations for larger times is more involved, since the maps  $T_1$  and  $T_2$  do not commute,

$$(T_2 T_1 - T_1 T_2)(x) = \frac{1}{2}(2x \bmod 1) - \left[ 2 \left( \frac{x}{2} \right) \bmod 1 \right] = \begin{cases} 0, & \text{if } x \in [0, \frac{1}{2}) \\ -\frac{1}{2}, & \text{if } x \in [\frac{1}{2}, 1] \end{cases}. \quad (18)$$

Thus, here we only provide the next two examples of exact values for  $k = 2, 3$ . By writing down all possibilities of the second iterate  $x_2$  we obtain (App. D)

$$\langle x_2 x_0 \rangle = \int_0^1 \rho(x_0) x_2 x_0 dx_0 = (2p-1) \left[ \frac{(3p+1)^2}{3(5p-1)} - \frac{11p+6}{16} \right]. \quad (19)$$

It can be easily checked that at  $p = 1$ ,  $\langle x_2 x_0 \rangle_{p=1} = 13/48$ , which is consistent with the result for the Bernoulli shift [89]. When  $k = 3$  we have (App. D)

$$\langle x_3 x_0 \rangle = \int_0^1 \rho(x_0) x_3 x_0 dx_0 = (2p-1) \left[ \frac{(3p+1)^3}{6(5p-1)} - \frac{28p^2 + 40p + 9}{32} \right]. \quad (20)$$

One can check again that this formula reproduces the result for the Bernoulli shift at  $p = 1$  [89]. In Fig. 5 we compare these three exact results with simulations. We see that the agreement is excellent, confirming the quality of our simulations.

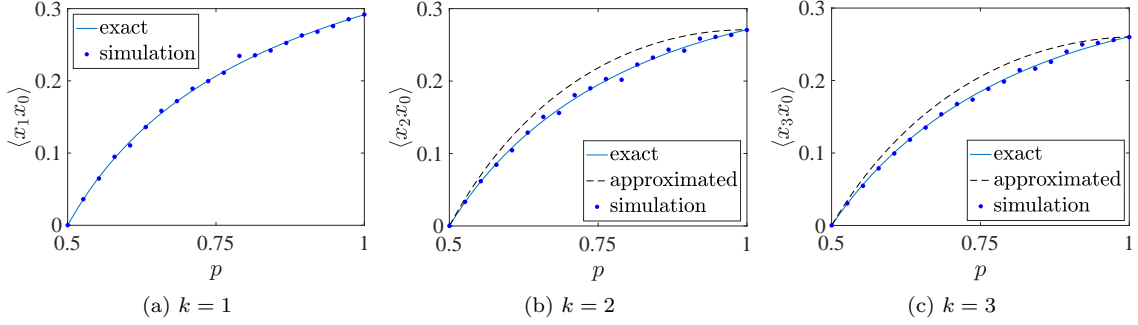


FIG. 5: Position autocorrelation function  $\langle x_k x_0 \rangle$  Eq. (16) for small times  $k = 1, 2, 3$ . In each plot, the solid curve represents the exact analytic result Eqns. (18), (19) and (20). The scattered points depict the simulation data for which  $10^5$  initial points have been sampled directly from the invariant density formula, with a truncation of 20 subintervals on the unit interval, where 20 equidistant values of  $p \in [0.5001, 0.9999]$  have been used. The two dashed curves show results from our analytical approximation Eqns. (22), (23).

### C. Analytical approximations for larger times

As explained in Sec. IIIB, the two maps defining the Pelikan map do not commute, see Eq. (18), hence the system is non-Markovian. However, the invariant density is highly concentrated on the subinterval  $x \in [0, 1/2)$  when  $p \rightarrow 1/2^+$ , where the commutator Eq. (18) is zero. In turn, for  $p \rightarrow 1$  the contraction  $T_2$  is randomly chosen less frequently, thus generating fewer combinations of  $T_i T_j$  ( $i \neq j$ ). For these two limiting regimes of  $p$  it is thus reasonable to approximate the original random system as if  $T_1$  and  $T_2$  were commutative, which is expected to yield a good qualitative approximation. In these situations we employ that iterates of the approximated map have a simple binomial structure. This enables us to derive analytically the autocorrelation function for a general time  $k \in \mathbb{N}$ . It should be noted, however, that our approach is only partially Markovian, in the sense that the original (non-commutative) dynamics is replaced by the Markovian dynamics. Yet, we are still assuming the same invariant density (i.e., the one for the actual non-commutative system).

First consider the second iteration of the approximated commutative system. It can take three possible values, namely

$$x_2 = \begin{cases} T_1(T_1(x_0)) = 4x_0 \mod 1, & \text{prob. } p^2 \\ T_i(T_j(x_0)) \simeq x_0, \quad i \neq j, & \text{prob. } 2p(1-p) \\ T_2(T_2(x_0)) = \frac{1}{4}x_0, & \text{prob. } (1-p)^2, \end{cases} \quad (21)$$

and thus (App. E)

$$\begin{aligned} \langle x_2 x_0 \rangle &\simeq p^2 \int_0^1 \rho_p(x_0) (4x_0 \mod 1) x_0 dx_0 + 2p(1-p) \int_0^1 \rho_p(x_0) x_0^2 dx_0 + (1-p)^2 \int_0^1 \rho_p(x_0) \frac{1}{4} x_0^2 dx_0 \\ &= (2p-1) \left[ \frac{(3p+1)^2}{3(5p-1)} - \frac{14p+3}{16} \right]. \end{aligned} \quad (22)$$

Similarly, we obtain

$$\langle x_3 x_0 \rangle \simeq (2p-1) \left[ \frac{(3p+1)^3}{6(5p-1)} - \frac{27p^2 + 47p + 3}{32} \right]. \quad (23)$$

Figure 5 compares these approximate results with both the exact and the numerical values for small times  $k = 1, 2, 3$ . We see that, the approximation qualitatively reproduces the functional form of the autocorrelation function under variation of  $p$ . As expected, the quantitative deviations are largest for intermediate values of  $p$  while the approximation works reasonably well for the limiting cases of  $p \rightarrow 1/2$  and  $p \rightarrow 1$ .

For general times  $k \in \mathbb{N}$ ,  $\langle x_k x_0 \rangle$  can be obtained by writing out all  $k + 1$  possible values of the  $k$ th iteration with corresponding binomial probabilities  $\binom{k}{j} p^j (1-p)^{k-j}$ ,  $j = 0, 1, \dots, k$ . A lengthy calculation yields [89]

$$\begin{aligned}
& \langle x_k x_0 \rangle(p) \\
& \simeq \frac{4(2p-1)}{3(5p-1)} \left( \frac{3p+1}{2} \right)^k \\
& - \frac{2p-1}{2} \left\{ \frac{8}{3(5p-1)} \left[ \left( \frac{3p+1}{2} \right)^k - (2p)^k \left( \frac{1-p}{4p} \right)^{K+1} \binom{k}{K+1} \cdot {}_2F_1 \left( a_1, a_2; b; -\frac{1-p}{4p} \right) \right] \right. \\
& - \frac{1}{3p-1} \left[ 1 - p^k \left( \frac{1-p}{p} \right)^{K+1} \binom{k}{K+1} \cdot {}_2F_1 \left( a_1, a_2; b; -\frac{1-p}{p} \right) \right] \\
& - \frac{1}{6(2p-1)} \left[ \left( \frac{4-3p}{2} \right)^k - \left( \frac{p}{2} \right)^k \left( \frac{4(1-p)}{p} \right)^{K+1} \binom{k}{K+1} \cdot {}_2F_1 \left( a_1, a_2; b; -\frac{4(1-p)}{p} \right) \right] \\
& \left. - \frac{(7p-3)(p-1)}{2(2p-1)(3p-1)(5p-1)} \left[ \left( \frac{3p+1}{2} \right)^k - \left( \frac{1-p}{2} \right)^k \left( \frac{4p}{1-p} \right)^{K+1} \binom{k}{K+1} \cdot {}_2F_1 \left( a_1, a_2; b; -\frac{4p}{1-p} \right) \right] \right\},
\end{aligned} \tag{24}$$

where  ${}_2F_1(a_1, a_2; b; x)$  is the Gauss hypergeometric function,  $a_1 = 1$ ,  $a_2 = -k + K + 1$ ,  $b = K + 2$  and,  $K = \frac{k}{2} - 1$  for even  $k$  and  $K = \frac{k-1}{2}$  for odd  $k$ . The difference for the results of odd and even  $k$  is due to the fact that, for even  $k$ , there is a possibility that the approximated map becomes the identity, where we have  $x_k = x_0$ . But for odd  $k$  this is impossible, as each odd iteration either expands or contracts the system.

We plot the results for the autocorrelation decay obtained from this formula in Fig. 6. We see in Fig. 6(a) that for  $p \rightarrow 1^-$  our analytical approximation correctly reproduces an exponential decay for odd and even  $k$ . This is consistent with the fact that for the Bernoulli shift (i.e.,  $p = 1$ ) we have precisely  $\langle \tilde{x}_k \tilde{x}_0 \rangle = (1/12) (1/2)^k$  [89, 95, 96]. In semi-logarithmic representation this yields a slope of  $\ln(1/2) \approx -0.69$ , which matches well to the results of our analytical approximation. Figure 6(b) confirms analytically the power-law correlation decay observed in our simulation results of Fig. 4(b).

We remark that at each iteration step in Eq. (24) a small deviation is made by this approximated approach compared to the exact Pelikan map. In the long run (i.e.,  $k \rightarrow \infty$ ) these errors will accumulate so that the exact results for the correlation decay of the Pelikan map will substantially deviate from this approximation. Our approximation is thus only valid for smaller times  $k$ , and in the two limits  $p \rightarrow 1/2^+$ ,  $p \rightarrow 1^-$ . When  $p$  is between these two limits, the non-commutativity of the Pelikan map plays an important role in the dynamics. How to better capture this property analytically is an interesting open question.

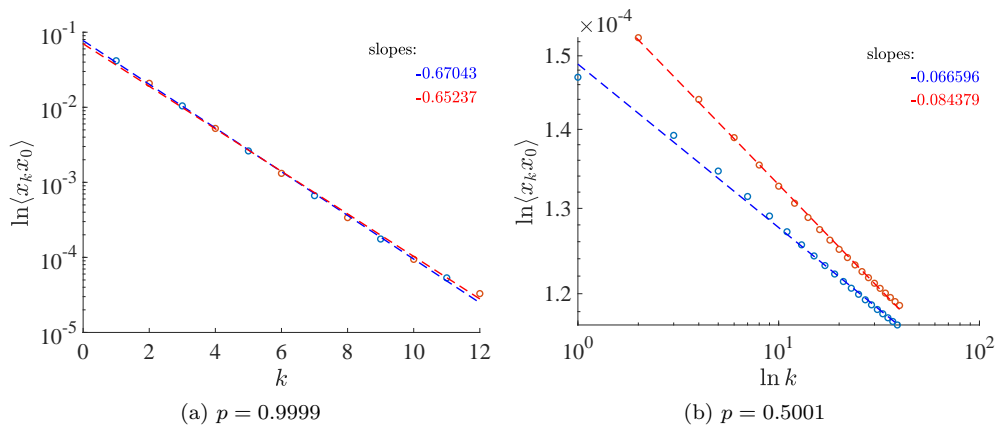


FIG. 6: Position autocorrelation functions  $\langle x_k x_0 \rangle$  Eq. (24) for (a)  $p = 0.9999$ ,  $k = 1, 2, \dots, 12$  (semi-logarithmic scale), (b)  $p = 0.5001$ ,  $k = 1, 2, \dots, 40$  (double-logarithmic scale). Odd times  $k$  are depicted in blue, even  $k$  in red. Dashed lines are linear fits with the slopes indicated on the top-right corner.

#### IV. CONCLUSION AND OUTLOOK

In this paper we studied a transition scenario that is generated by a class of simple random dynamical systems, i.e., piecewise linear one-dimensional maps, where we focused on the Pelikan map. This particular model stands out as one of the rare examples that can be understood analytically for the entire range of parameter values. The transition exhibited by it also stands out, because it is of particular interest to learn how a typical transition scenario looks like in a system where a parameter is changed that controls the relative likelihood by which an expanding dynamics is chosen as compared to a contracting one [28].

To characterise this transition, we first derived analytically the coarse-grained invariant density of the Pelikan map and found that it undergoes multiple transitions under parameter variation, such as changes in convexity, boundedness and normalisability. All these critical behaviours can be extended to a broader family of random maps that includes the Pelikan map as a special case. Secondly, we provided numerical evidence for weak ergodicity breaking at the critical parameter value where the normalisation of the invariant density changes from finite to infinite. This was demonstrated by an inequality between time and ensemble average of the position as an observable. Thirdly, we studied the position autocorrelation function both numerically and analytically. Our findings unveiled a transition from exponential to power-law decay under parameter variation, indicating the emergence of anomalous dynamics at the transition point. Overall, our study thus provides a comprehensive examination of the complete dynamical transition in the Pelikan map under variation of the sampling probability as a parameter. Characteristic properties such as critical density changes, weak ergodicity breaking and anomalous correlation decay are expected to be observed in other, more complex dynamical systems as well.

There are many interesting open questions. Perhaps the most important one is the derivation of an exact analytical expression for the position autocorrelation function of the Pelikan map at the transition point for all times, respectively a mathematical proof of its decay in the limit of long times. To answer this question it would be interesting to explore more sophisticated methods expressing the correlation function in terms of eigenvalues and eigenfunctions of the Frobenius-Perron operator of the random map, by then solving the associated eigenvalue problem, as has been accomplished for simpler deterministic maps [95]. Although many features of the Pelikan map can be analytically understood more easily, this particular problem turned out to be very difficult because of the non-commuting properties that we highlighted in Sec. III B. Notably, many phenomena in quantum systems involve non-commuting operators, so from this point of view it would be interesting to make further progress in this direction. This would be particularly significant in the realm of other non-commutative dynamical systems as well, being quantum mechanical or just classical, as long as they include a random sampling of different dynamics where the order of the choice is relevant.

It would also be interesting to further employ this class of maps for defining associated diffusive dynamical systems. This has already been done for a particular setting in Ref. [28] by delivering an interesting transition from normal to anomalous (sub)diffusion. However, it would be important to study yet other types of diffusive random dynamical systems. Especially, obtaining one that generates superdiffusion is currently an open question. In Ref. [91] a deterministic Langevin dynamics has been proposed, where the iterates of a simple one-dimensional map are used as the fast driving force for a slowly changing dissipative dynamics. In other words, the Gaussian white noise of an ordinary Langevin equation has been replaced by a more complex dynamical systems noise source, for which also the Pelikan map could be used. This spatially extended dynamical systems would be diffusive and would allow us to investigate the influence of the transition controlled by the sampling probability of the Pelikan map onto a corresponding diffusion processes (defined, in the simplest case, by the variable  $y_n$  as given in Eq. (14)). It has been suggested that strongly chaotic behaviour in dynamical systems generates normal diffusion, whereas non-stationary intermittency (or weakly chaotic dynamics) yields anomalous diffusion [28, 66]. A diffusive dynamical system driven by the Pelikan map would thus provide an interesting test ground to further investigate these types of questions. Our observations reported in this paper indicate that in the vicinity of the critical point, represented by the parameter value where the Lyapunov exponent is zero, the decay of the position autocorrelation function behaves anomalously. Correspondingly, an associated diffusive random dynamical system should generically display a transition to anomalous diffusion.

So far, our investigations have focused solely on one-dimensional random maps. However, it is worth noting that higher-dimensional random dynamical systems of the same type can also be defined, such as, e.g., iterated function systems [98], which may exhibit significantly more complex transitions. Exploring higher-dimensional random dynamical systems could potentially provide deeper insights into more complex real-world systems. For such an endeavour the Pelikan map promises to serve as an important guideline, in the form of a low-dimensional example where many generic phenomena can already be understood in detail.

**Acknowledgement:** The authors thank the London Mathematical Laboratory for financial support and the initialisation of this project in the form of two Summer Schools at the ICTP Trieste in 2019 and 2021. Here YS, SR and RK worked together with JY and MM during one-month Summer projects, leading to the present results. RK and YS thank Prof. A.J.Homburg for discussions, which started at a workshop in 2019 where we presented our

work Ref. [28], as well as for making them aware of Refs. [74, 90]. RK also thanks Dr. W.Just, Dr. M.Rasmussen and Prof. J.S.W.Lamb for hints on relevant literature and many helpful remarks.

### Appendix A: Derivation of the invariant density curve formula

For  $p \in (\frac{1}{2}, 1]$ , the invariant density is normalisable, i.e., we have  $\sum_{i=0}^{\infty} r_i = 1$ ,

$$\begin{aligned}
1 &= \lim_{n \rightarrow \infty} (r_0 + r_1 + \dots + r_n) \\
&= \lim_{n \rightarrow \infty} \left( \frac{1}{2} a_0 + \frac{1}{2^2} R_1 a_0 + \dots + \frac{1}{2^{n+1}} R_n \cdot R_{n-1} \cdot \dots \cdot R_1 a_0 \right) \\
&= \frac{a_0}{2} \lim_{n \rightarrow \infty} \left( 1 + \frac{1}{2} R_1 + \frac{1}{2^2} R_2 R_1 + \dots + \frac{1}{2^n} R_n \cdot \dots \cdot R_1 \right) \\
&= \frac{a_0}{-1 + \frac{2(1-p)}{p}} \lim_{n \rightarrow \infty} \left( -\frac{1}{2} + \frac{1-p}{p} - \frac{1}{4} \sum_{i=0}^{n-1} \left( \frac{1}{2} \right)^i + \left( \frac{1-p}{p} \right)^2 \sum_{i=0}^{n-1} \left( \frac{1-p}{p} \right)^{n-1-i} \right) \\
&= \frac{a_0}{-1 + \frac{2(1-p)}{p}} \left( -\frac{1}{2} + \frac{1-p}{p} - \frac{1}{4} \cdot \frac{1}{1 - \frac{1}{2}} + \left( \frac{1-p}{p} \right)^2 \cdot \frac{1}{1 - \frac{1-p}{p}} \right) \\
&= \frac{a_0 p}{2p-1},
\end{aligned}$$

where from the second line onwards we have denoted

$$R_n = R_n(p) := \frac{a_n}{a_{n-1}} = 2 \frac{r_n}{r_{n-1}} = \frac{-1 + \left( \frac{2(1-p)}{p} \right)^{n+1}}{-1 + \left( \frac{2(1-p)}{p} \right)^n}.$$

Therefore,

$$a_0 = \frac{2p-1}{p}, \quad p \in \left( \frac{1}{2}, 1 \right].$$

By the recurrence relation of  $\{a_n\}$  we have an explicit form for the amplitude

$$a_n = \frac{-1 + \left( \frac{2(1-p)}{p} \right)^{n+1}}{-1 + \frac{2(1-p)}{p}} a_0 = \frac{2p-1}{2-3p} \left[ -1 + \left( \frac{2(1-p)}{p} \right)^{n+1} \right]. \quad (\text{A1})$$

The invariant density curve is given by the mid-point interpolation  $(\frac{3}{2^{n+2}}, a_n)$ , and with Eq. (A1),

$$\begin{aligned}
x = \frac{3}{2^{n+2}} &\Rightarrow n+1 = \log_2 \frac{3}{2x} = \frac{\ln 3}{\ln 2} - 1 - \frac{\ln x}{\ln 2}, \\
\tilde{\rho}_p(x) &= \frac{2p-1}{3p-2} \left[ 1 - \left( \frac{2(1-p)}{p} \right)^{n+1} \right] \\
&= \frac{2p-1}{3p-2} \left[ 1 - \left( \frac{2(1-p)}{p} \right)^{\frac{\ln 3}{\ln 2} - 1 - \frac{\ln x}{\ln 2}} \right] \\
&= \frac{2p-1}{3p-2} \left[ 1 - \left( \frac{2(1-p)}{p} \right)^{\frac{\ln 3}{\ln 2} - 1} \left( \frac{p}{2(1-p)} \right)^{\frac{\ln x}{\ln 2}} \right] \\
&= \frac{2p-1}{3p-2} \left[ 1 - \left( \frac{2(1-p)}{p} \right)^{\frac{\ln 3}{\ln 2} - 1} e^{\frac{\ln x}{\ln 2} \ln \frac{1}{2}} \left( \frac{p}{1-p} \right)^{\frac{\ln x}{\ln 2}} \right] \\
&= \frac{2p-1}{3p-2} \left[ 1 - \left( \frac{2(1-p)}{p} \right)^{\frac{\ln 3}{\ln 2} - 1} x^{-1} e^{\ln x \frac{1}{\ln 2} \ln \frac{p}{1-p}} \right] \\
&= \frac{2p-1}{3p-2} \left[ 1 - \left( \frac{2(1-p)}{p} \right)^{\frac{\ln 3}{\ln 2} - 1} x^{-1 + \frac{1}{\ln 2} \ln \frac{p}{1-p}} \right] \\
&=: A(1 - Bx^{-1+C}), \\
\text{where } A(p) &:= \frac{2p-1}{3p-2}, B(p) := \left( \frac{2(1-p)}{p} \right)^{\frac{\ln 3}{\ln 2} - 1}, C(p) := \frac{1}{\ln 2} \ln \frac{p}{1-p}.
\end{aligned}$$

### Appendix B: Derivation of the convexity change for a general case

The method follows directly from Ref. [24] except that the expansion rate is any integer  $s \geq 2$ . Analogous to Eq.(3), for  $s_1 = s = 1/s_2$  we have

$$\frac{r_{n+1}}{r_n} = \frac{-1 + \left( \frac{s(1-p)}{p} \right)^{n+2}}{-s + s \left( \frac{s(1-p)}{p} \right)^{n+1}}. \quad (\text{B1})$$

The normalisation condition

$$1 = \sum_{j=0}^{\infty} r_j = \lim_{n \rightarrow \infty} (r_0 + r_1 + \dots + r_n) = a_0 \frac{p}{(s-1)(2p-1)} \quad (\text{B2})$$

gives  $a_0 = \frac{(s-1)(2p-1)}{p}$  and therefore

$$a_n = \frac{-1 + \left( \frac{s(1-p)}{p} \right)^{n+1}}{-1 + \frac{s(1-p)}{p}} a_0 = \frac{(s-1)(2p-1)}{s - (s+1)p} \left[ -1 + \left( \frac{s(1-p)}{p} \right)^{n+1} \right]. \quad (\text{B3})$$

By mid-point interpolation  $(\frac{s+1}{2s^{n+1}}, a_n)$  (cf. Sec. A) we get

$$\tilde{\rho}_p(x) = A_s(1 - B_s x^{-1+C_s}), \quad (\text{B4})$$

where

$$A_s(p) = \frac{(s-1)(2p-1)}{(s+1)p - s}, \quad B_s(p) = \left( \frac{s(1-p)}{p} \right)^{\frac{\ln(s+1)}{\ln s} - \frac{\ln 2}{\ln s}}, \quad C_s(p) = \frac{1}{\ln s} \ln \frac{p}{1-p}. \quad (\text{B5})$$

When  $s = 2$  we recover the Pelikan case. The convexity changes when  $C_s = 2$ , which gives the critical value of  $p$ :  $p_c = \frac{s^2}{1+s^2}$ .

### Appendix C: Derivation of the moments of the Pelikan map

The  $m$ th moment is given by the expectation of  $x^m$  with respect to the invariant density  $\rho_p(x)$  of the Pelikan map [89],

$$\begin{aligned}
\langle x^m \rangle &= \int_0^1 \rho_p(x) x^m dx \\
&= \sum_{j=0}^{\infty} a_j \int_{\frac{1}{2^{j+1}}}^{\frac{1}{2^j}} x^m dx \\
&= \frac{1}{m+1} \sum_{j=0}^{\infty} a_j \left( \frac{1}{2^{j(m+1)}} - \frac{1}{2^{(j+1)(m+1)}} \right) \\
&= \frac{1}{m+1} \cdot \left( 1 - \frac{1}{2^{m+1}} \right) \sum_{j=0}^{\infty} a_j \left( \frac{1}{2^{m+1}} \right)^j \\
&= \frac{1}{m+1} \cdot \left( 1 - \frac{1}{2^{m+1}} \right) \cdot \frac{2p-1}{3p-2} \sum_{j=0}^{\infty} \left[ 1 - \left( \frac{2(1-p)}{p} \right)^{j+1} \right] \left( \frac{1}{2^{m+1}} \right)^j \\
&= \frac{1}{m+1} \cdot \left( 1 - \frac{1}{2^{m+1}} \right) \cdot \frac{2p-1}{3p-2} \left[ \sum_{j=0}^{\infty} \left( \frac{1}{2^{m+1}} \right)^j - \frac{2(1-p)}{p} \sum_{j=0}^{\infty} \left( \frac{1-p}{2^m p} \right)^j \right] \\
&= \frac{1}{m+1} \cdot \frac{2^{m+1}-1}{2^{m+1}} \cdot \frac{2p-1}{3p-2} \left[ \frac{2^{m+1}}{2^{m+1}-1} - \frac{2^{m+1}(1-p)}{2^m p - 1 + p} \right] \\
&= \frac{1}{m+1} \cdot \frac{2p-1}{3p-2} \cdot \frac{2^m(3p-2)}{2^m p - 1 + p} \\
&= \frac{2^m}{m+1} \cdot \frac{2p-1}{(2^m+1)p-1}.
\end{aligned}$$

In particular, when  $m = 1$ , the average of  $x$  reads

$$\langle x \rangle = \frac{2p-1}{3p-1},$$

and when  $m = 2$ ,

$$\langle x^2 \rangle = \frac{4(2p-1)}{3(5p-1)}.$$

### Appendix D: Derivation of the exact auto-correlation functions of time differences $k = 2$ and 3

The second iterate of  $x$  can take different values with their corresponding probabilities:

$$x_2 = \begin{cases} T_1(T_1(x_0)) = 4x_0 \bmod 1 = \begin{cases} 4x_0, & x_0 \in [0, \frac{1}{4}) \\ 4x_0 - 1, & x_0 \in [\frac{1}{4}, \frac{1}{2}) \\ 4x_0 - 2, & x_0 \in [\frac{1}{2}, \frac{3}{4}) \\ 4x_0 - 3, & x_0 \in [\frac{3}{4}, 1] \end{cases}, & \text{prob. } p^2 \\ T_2(T_1(x_0)) = \frac{1}{2}(2x_0 \bmod 1) = \begin{cases} x_0, & x_0 \in [0, \frac{1}{2}) \\ x_0 - \frac{1}{2}, & x_0 \in [\frac{1}{2}, 1] \end{cases}, & \text{prob. } (1-p)p \\ T_1(T_2(x_0)) = x_0, & \text{prob. } p(1-p) \\ T_2(T_2(x_0)) = \frac{1}{4}x_0, & \text{prob. } (1-p)^2 \end{cases} \quad (\text{D1})$$



Therefore,

$$\begin{aligned}
\langle x_2 x_0 \rangle &= \int_0^1 \rho(x_0) x_2 x_0 dx_0 \\
&= p^2 \int_0^1 \rho(x) (4x \bmod 1) x dx + p(1-p) \left[ \int_0^{\frac{1}{2}} \rho(x) x^2 dx + \int_{\frac{1}{2}}^1 \rho(x) (x - \frac{1}{2}) x dx \right] \\
&\quad + p(1-p) \int_0^1 \rho(x) x^2 dx + (1-p)^2 \int_0^1 \rho(x) \frac{1}{4} x^2 dx \\
&= p^2 \left[ \int_0^{\frac{1}{4}} \rho(x) 4x^2 dx + \int_{\frac{1}{4}}^{\frac{2}{4}} \rho(x) (4x-1) x dx + \int_{\frac{2}{4}}^{\frac{3}{4}} \rho(x) (4x-2) x dx + \int_{\frac{3}{4}}^1 \rho(x) (4x-3) x dx \right] + \\
&\quad + p(1-p) \left[ \int_0^{\frac{1}{2}} \rho(x) x^2 dx + \int_{\frac{1}{2}}^1 \rho(x) (x^2 - \frac{1}{2}x) dx \right] + p(1-p) \langle x^2 \rangle + \frac{(1-p)^2}{4} \langle x^2 \rangle \\
&= 4p^2 \langle x^2 \rangle - p^2 \left[ \int_{\frac{1}{4}}^{\frac{2}{4}} \rho(x) x dx + 2 \int_{\frac{2}{4}}^{\frac{3}{4}} \rho(x) x dx + 3 \int_{\frac{3}{4}}^1 \rho(x) x dx \right] + p(1-p) \left[ \langle x^2 \rangle - \frac{1}{2} \int_{\frac{1}{2}}^1 \rho(x) x dx \right] \\
&\quad + p(1-p) \langle x^2 \rangle + \frac{(1-p)^2}{4} \langle x^2 \rangle \\
&= \left( 4p^2 + 2p(1-p) + \frac{(1-p)^2}{4} \right) \langle x^2 \rangle - p^2 \left[ a_1 \frac{x^2}{2} \Big|_{\frac{1}{4}}^{\frac{2}{4}} + 2a_0 \frac{x^2}{2} \Big|_{\frac{2}{4}}^{\frac{3}{4}} + 3a_0 \frac{x^2}{2} \Big|_{\frac{3}{4}}^1 \right] - \frac{p(1-p)}{2} a_0 \frac{x^2}{2} \Big|_{\frac{1}{2}}^1 \\
&= \frac{(3p+1)^2}{4} \langle x^2 \rangle - p^2 \left[ \frac{(2p-1)(2-p)}{2p^2} \frac{4-1}{16} + 2 \frac{2p-1}{2p} \frac{9-4}{16} + 3 \frac{2p-1}{2p} \frac{16-9}{16} \right] - \frac{p(1-p)}{4} \frac{2p-1}{p} \frac{4-1}{4} \\
&= \frac{(3p+1)^2}{4} \frac{4(2p-1)}{3(5p-1)} - \frac{(2p-1)(14p+3)}{16} - \frac{3(2p-1)(1-p)}{16} \\
&= (2p-1) \left[ \frac{(3p+1)^2}{3(5p-1)} - \frac{11p+6}{16} \right].
\end{aligned}$$

The third iteration of the Pelikan map reads

$$x_3 = \begin{cases} \begin{cases} T_1 T_1 T_1(x_0) = 8x_0 \bmod 1 = [8 \text{ cases}], & \text{prob. } p^3 \\ T_2 T_1 T_1(x_0) = \frac{1}{2}(4x_0 \bmod 1) = \begin{cases} \frac{1}{2}(4x_0) = 2x_0, & x_0 \in [0, \frac{1}{4}) \\ \frac{1}{2}(4x_0 - 1) = 2x_0 - \frac{1}{2}, & x_0 \in [\frac{1}{4}, \frac{1}{2}) \\ \frac{1}{2}(4x_0 - 2) = 2x_0 - 1, & x_0 \in [\frac{1}{2}, \frac{3}{4}) \\ \frac{1}{2}(4x_0 - 3) = 2x_0 - \frac{3}{2}, & x_0 \in [\frac{3}{4}, 1] \end{cases}, & \text{prob. } (1-p)p^2 \end{cases} \\ \begin{cases} T_1 T_2 T_1(x_0) = 2x_0 \bmod 1 = [2 \text{ cases}], & \text{prob. } p(1-p)p \\ T_2 T_2 T_1(x_0) = \frac{1}{4}(2x_0 \bmod 1) = \begin{cases} \frac{1}{2}x_0, & x_0 \in [0, \frac{1}{2}) \\ \frac{1}{2}x_0 - \frac{1}{4}, & x_0 \in [\frac{1}{2}, 1] \end{cases}, & \text{prob. } (1-p)^2 p \end{cases} \\ \begin{cases} T_1 T_1 T_2(x_0) = 2x_0 \bmod 1 = [2 \text{ cases}], & \text{prob. } p^2(1-p) \\ T_2 T_1 T_2(x_0) = \frac{1}{2}x_0, & \text{prob. } (1-p)p(1-p) \\ T_1 T_2 T_2(x_0) = \frac{1}{2}x_0, & \text{prob. } p(1-p)^2 \\ T_2 T_2 T_2(x_0) = \frac{1}{8}x_0, & \text{prob. } (1-p)^3 \end{cases} \end{cases}
\end{cases}$$

which gives

$$\begin{aligned}
\langle x_3 x_0 \rangle &= \int_0^1 \rho(x_0) x_3 x_0 dx_0 \\
&= p^3 \int_0^1 \rho(x) (8x \bmod 1) x dx + p^2(1-p) \left[ \int_0^{\frac{1}{4}} \rho(x) 2x^2 dx + \int_{\frac{1}{4}}^{\frac{1}{2}} \rho(x) (2x - \frac{1}{2}) x dx + \int_{\frac{1}{2}}^{\frac{3}{4}} \rho(x) (2x - 1) x dx \right. \\
&\quad \left. + \int_{\frac{3}{4}}^1 \rho(x) (2x - \frac{3}{2}) x dx \right] + 2p^2(1-p) \int_0^1 \rho(x) (2x \bmod 1) x dx + p(1-p)^2 \left[ \int_0^{\frac{1}{2}} \rho(x) \frac{1}{2} x^2 dx + \int_{\frac{1}{2}}^1 \rho(x) (\frac{1}{2}x - \frac{1}{4}) x dx \right] \\
&\quad + 2p(1-p)^2 \int_0^1 \rho(x) \frac{1}{2} x^2 dx + (1-p)^3 \int_0^1 \rho(x) \frac{1}{8} x^2 dx \\
&= p^3 \left[ 8\langle x^2 \rangle - \int_{\frac{1}{8}}^{\frac{2}{8}} \rho(x) x dx - 2 \int_{\frac{2}{8}}^{\frac{3}{8}} \rho(x) x dx - \int_{\frac{3}{8}}^{\frac{4}{8}} 3\rho(x) x dx - 4 \int_{\frac{4}{8}}^{\frac{5}{8}} \rho(x) x dx - 5 \int_{\frac{5}{8}}^{\frac{6}{8}} \rho(x) x dx - 6 \int_{\frac{6}{8}}^{\frac{7}{8}} \rho(x) x dx \right. \\
&\quad \left. - 7 \int_{\frac{7}{8}}^1 \rho(x) x dx \right] + p^2(1-p) \left[ 2\langle x^2 \rangle - \frac{1}{2} \int_{\frac{1}{4}}^{\frac{1}{2}} \rho(x) x dx - \int_{\frac{1}{2}}^{\frac{3}{4}} \rho(x) x dx - \frac{3}{2} \int_{\frac{3}{4}}^1 \rho(x) dx \right] \\
&\quad + 2p^2(1-p) \left[ 2\langle x^2 \rangle - \int_{\frac{1}{2}}^1 \rho(x) x dx \right] + p(1-p)^2 \left[ \frac{1}{2} \langle x^2 \rangle - \frac{1}{4} \int_{\frac{1}{2}}^1 \rho(x) x dx \right] + p(1-p)^2 \langle x^2 \rangle + \frac{(1-p)^3}{8} \langle x^2 \rangle \\
&= \left( 8p^3 + 2p^2(1-p) + 4p^2(1-p) + \frac{p(1-p)^2}{2} + p(1-p)^2 + \frac{(1-p)^3}{8} \right) \langle x^2 \rangle \\
&\quad - p^3 \left[ a_2 \frac{x^2}{2} \Big|_{\frac{1}{8}}^{\frac{2}{8}} + 2a_1 \frac{x^2}{2} \Big|_{\frac{2}{8}}^{\frac{3}{8}} + 3a_1 \frac{x^2}{2} \Big|_{\frac{3}{8}}^{\frac{4}{8}} + 4a_0 \frac{x^2}{2} \Big|_{\frac{4}{8}}^{\frac{5}{8}} + 5a_0 \frac{x^2}{2} \Big|_{\frac{5}{8}}^{\frac{6}{8}} + 6a_0 \frac{x^2}{2} \Big|_{\frac{6}{8}}^{\frac{7}{8}} + 7a_0 \frac{x^2}{2} \Big|_{\frac{7}{8}}^1 \right] \\
&\quad - p^2(1-p) \left[ \frac{a_1}{2} \frac{x^2}{2} \Big|_{\frac{1}{4}}^{\frac{1}{2}} + a_0 \frac{x^2}{2} \Big|_{\frac{1}{2}}^{\frac{3}{4}} + \frac{3a_0}{2} \frac{x^2}{2} \Big|_{\frac{3}{4}}^1 \right] - 2p^2(1-p)a_0 \frac{x^2}{2} \Big|_{\frac{1}{2}}^1 - \frac{p(1-p)^2}{4} a_0 \frac{x^2}{2} \Big|_{\frac{1}{2}}^1 \\
&= \frac{(3p+1)^3}{8} \frac{4(2p-1)}{3(5p-1)} - \frac{p^3}{2} \left[ \frac{(2p-1)(3p^2-6p+4)}{p^3} \frac{3}{64} + \frac{(2p-1)(2-p)}{p^2} \left( \frac{2 \cdot 5}{64} + \frac{3 \cdot 7}{64} \right) \right. \\
&\quad \left. + \frac{(2p-1)}{p} \left( \frac{4 \cdot 9}{64} + \frac{5 \cdot 11}{64} + \frac{6 \cdot 13}{64} + \frac{7 \cdot 15}{64} \right) \right] - \frac{p^2(1-p)}{4} \left[ \frac{(2p-1)(2-p)}{p^2} \frac{3}{16} + \frac{(2p-1)}{p} \left( \frac{2 \cdot 5}{16} + \frac{3 \cdot 7}{16} \right) \right] \\
&\quad - \left( p^2(1-p) \frac{2p-1}{p} + \frac{p(1-p)^2}{8} \frac{2p-1}{p} \right) \frac{3}{4} \\
&= \frac{(2p-1)(3p+1)^3}{6(5p-1)} - \frac{(2p-1)(63p^2+11p+3)}{32} - \frac{(2p-1)(1-p)(14p+3)}{32} - \frac{3(2p-1)(1-p)(7p+1)}{32} \\
&= (2p-1) \left[ \frac{(3p+1)^3}{6(5p-1)} - \frac{28p^2+40p+9}{32} \right].
\end{aligned}$$

**Appendix E: Derivation of the approximated auto-correlation functions of time differences  $k = 2$  and 3**

$$\begin{aligned}
\langle x_2 x_0 \rangle &\simeq p^2 \int_0^1 \rho_p(x_0) (4x_0 \bmod 1) x_0 dx_0 + 2p(1-p) \int_0^1 \rho_p(x_0) x_0^2 dx_0 + (1-p)^2 \int_0^1 \rho_p(x_0) \frac{1}{4} x_0^2 dx_0 \\
&= p^2 \left[ \int_0^{\frac{1}{4}} \rho_p(x_0) 4x_0^2 dx_0 + \int_{\frac{1}{4}}^{\frac{1}{2}} \rho_p(x_0) (4x_0 - 1) x_0 dx_0 + \int_{\frac{1}{2}}^{\frac{3}{4}} \rho_p(x_0) (4x_0 - 2) x_0 dx_0 \right. \\
&\quad \left. + \int_{\frac{3}{4}}^1 \rho_p(x_0) (4x_0 - 3) x_0 dx_0 \right] + 2p(1-p) \langle x^2 \rangle + \frac{(1-p)^2}{4} \langle x^2 \rangle \\
&= p^2 \left[ \int_0^1 \rho_p(x_0) 4x_0^2 dx_0 - \int_{\frac{1}{4}}^{\frac{1}{2}} \rho_p(x_0) x_0 dx_0 - 2 \int_{\frac{1}{2}}^{\frac{3}{4}} \rho_p(x_0) x_0 dx_0 - 3 \int_{\frac{3}{4}}^1 \rho_p(x_0) x_0 dx_0 \right] + \left[ 2p(1-p) + \frac{(1-p)^2}{4} \right] \langle x^2 \rangle \\
&= \left[ 4p^2 + 2p(1-p) + \frac{(1-p)^2}{4} \right] \langle x^2 \rangle - p^2 \left[ a_1 \int_{\frac{1}{4}}^{\frac{1}{2}} x dx + 2a_0 \int_{\frac{1}{2}}^{\frac{3}{4}} x dx + 3a_0 \int_{\frac{3}{4}}^1 x dx \right] \\
&= \frac{(3p+1)^2}{4} \langle x^2 \rangle - p^2 \left[ \frac{(2p-1)(2-p)}{p^2} \cdot \frac{3}{32} + 2 \cdot \frac{2p-1}{p} \cdot \frac{5}{32} + 3 \cdot \frac{2p-1}{p} \cdot \frac{7}{32} \right] \\
&= \frac{(3p+1)^2}{4} \cdot \frac{4(2p-1)}{3(5p-1)} - \left[ \frac{3(2p-1)(2-p)}{32} + \frac{5p(2p-1)}{16} + \frac{21p(2p-1)}{32} \right] \\
&= (2p-1) \left[ \frac{(3p+1)^2}{3(5p-1)} - \frac{14p+3}{16} \right].
\end{aligned}$$

The third iteration of the approximated system is given by

$$x_3 = \begin{cases} T_1(T_1(T_1(x_0))) = 2^3 x_0 \bmod 1, & \text{prob. } p^3 \\ T_i(T_j(T_k(x_0))) = 2x_0 \bmod 1, & \text{only one of } i, j, k \text{ is 1, prob. } 3p^2(1-p) \\ T_i(T_j(T_k(x_0))) = \frac{1}{2}x_0, & \text{only one of } i, j, k \text{ is 2, prob. } 3p(1-p)^2 \\ T_2(T_2(T_2(x_0))) = \frac{1}{2^3}x_0, & \text{prob. } (1-p)^3, \end{cases}$$

and

$$\begin{aligned}
\langle x_3 x_0 \rangle &\simeq p^3 \int_0^1 \rho_p(x_0) (8x_0 \bmod 1) x_0 dx_0 + 3p^2(1-p) \int_0^1 \rho_p(x_0) (2x_0 \bmod 1) x_0 dx_0 + 3p(1-p)^2 \int_0^1 \rho_p(x_0) \frac{1}{2} x_0^2 dx_0 \\
&\quad + (1-p)^3 \int_0^1 \rho_p(x_0) \frac{1}{8} x_0^3 dx_0 \\
&= p^3 \left[ \int_0^{\frac{1}{8}} \rho_p(x_0) 8x_0^2 dx_0 + \int_{\frac{1}{8}}^{\frac{2}{8}} \rho_p(x_0) (8x_0 - 1) x_0 dx_0 + \int_{\frac{2}{8}}^{\frac{3}{8}} \rho_p(x_0) (8x_0 - 2) x_0 dx_0 + \int_{\frac{3}{8}}^{\frac{4}{8}} \rho_p(x_0) (8x_0 - 3) x_0 dx_0 \right. \\
&\quad \left. \int_{\frac{4}{8}}^{\frac{5}{8}} \rho_p(x_0) (8x_0 - 4) x_0 dx_0 + \int_{\frac{5}{8}}^{\frac{6}{8}} \rho_p(x_0) (8x_0 - 5) x_0 dx_0 + \int_{\frac{6}{8}}^{\frac{7}{8}} \rho_p(x_0) (8x_0 - 6) x_0 dx_0 + \int_{\frac{7}{8}}^1 \rho_p(x_0) (8x_0 - 7) x_0 dx_0 \right] \\
&\quad + 3p^2(1-p) \left[ \int_0^{\frac{1}{2}} 2x_0^2 dx_0 + \int_{\frac{1}{2}}^1 (2x_0 - 1) x_0 dx_0 \right] + \frac{3p(1-p)^2}{2} \langle x^2 \rangle + \frac{(1-p)^3}{8} \langle x^2 \rangle \\
&= p^3 \left[ 8 \int_0^1 \rho_p(x_0) x_0^2 dx_0 - \int_{\frac{1}{8}}^{\frac{2}{8}} \rho_p(x_0) x_0 dx_0 - 2 \int_{\frac{2}{8}}^{\frac{3}{8}} \rho_p(x_0) x_0 dx_0 - 3 \int_{\frac{3}{8}}^{\frac{4}{8}} \rho_p(x_0) x_0 dx_0 - 4 \int_{\frac{4}{8}}^{\frac{5}{8}} \rho_p(x_0) x_0 dx_0 \right. \\
&\quad \left. - 5 \int_{\frac{5}{8}}^{\frac{6}{8}} \rho_p(x_0) x_0 dx_0 - 6 \int_{\frac{6}{8}}^{\frac{7}{8}} \rho_p(x_0) x_0 dx_0 - 7 \int_{\frac{7}{8}}^1 \rho_p(x_0) x_0 dx_0 \right] + 3p^2(1-p) \left[ 2 \int_0^1 \rho_p(x_0) x_0^2 dx_0 - \int_{\frac{1}{2}}^1 \rho_p(x_0) x_0 dx_0 \right] \\
&\quad + \left[ \frac{3p(1-p)^2}{2} + \frac{(1-p)^3}{8} \right] \langle x^2 \rangle \\
&= \left[ 8p^3 + 3p^2(1-p) + \frac{3p(1-p)^2}{2} + \frac{(1-p)^3}{8} \right] \langle x^2 \rangle - p^3 \left[ a_2 \int_{\frac{1}{8}}^{\frac{2}{8}} x dx + 2a_1 \int_{\frac{2}{8}}^{\frac{3}{8}} x dx + 3a_1 \int_{\frac{3}{8}}^{\frac{4}{8}} x dx + 4a_0 \int_{\frac{4}{8}}^{\frac{5}{8}} x dx \right. \\
&\quad \left. + 5a_0 \int_{\frac{5}{8}}^{\frac{6}{8}} x dx + 6a_0 \int_{\frac{6}{8}}^{\frac{7}{8}} x dx + 7a_0 \int_{\frac{7}{8}}^1 x dx \right] - 3p^2(1-p)a_0 \int_{\frac{1}{2}}^1 x dx \\
&= \left( 2p + \frac{(1-p)}{2} \right)^3 \langle x^2 \rangle - p^3 \left[ \frac{(2p-1)(3p^2-6p+4)}{p^3} \cdot \frac{3}{128} + 2 \cdot \frac{(2p-1)(2-p)}{p^2} \cdot \frac{5}{128} + 3 \cdot \frac{(2p-1)(2-p)}{p^2} \cdot \frac{7}{128} \right. \\
&\quad \left. + 4 \cdot \frac{2p-1}{p} \cdot \frac{9}{128} + 5 \cdot \frac{2p-1}{p} \cdot \frac{11}{128} + 6 \cdot \frac{2p-1}{p} \cdot \frac{13}{128} + 7 \cdot \frac{2p-1}{p} \cdot \frac{15}{128} \right] - 3p^2(1-p) \cdot \frac{2p-1}{p} \cdot \frac{3}{8} \\
&= \frac{(3p+1)^3}{8} \frac{4(2p-1)}{3(5p-1)} - \left[ \frac{3(2p-1)(3p^2-6p+4)}{128} + \frac{10p(2p-1)(2-p)}{128} + \frac{21p(2p-1)(2-p)}{128} + \frac{36p^2(2p-1)}{128} \right. \\
&\quad \left. + \frac{55p^2(2p-1)}{128} + \frac{78p^2(2p-1)}{128} + \frac{105p^2(2p-1)}{128} \right] - \frac{9p(1-p)(2p-1)}{8} \\
&= (2p-1) \left[ \frac{(3p+1)^3}{6(5p-1)} - \frac{63p^2+11p+3}{32} - \frac{9p(1-p)}{8} \right] \\
&= (2p-1) \left[ \frac{(3p+1)^3}{6(5p-1)} - \frac{27p^2+47p+3}{32} \right].
\end{aligned}$$

- 
- [1] A. Katok and B. Hasselblatt, *Introduction to the modern theory of dynamical systems*, Encyclopedia of Mathematics and its Applications, Vol. 54 (Cambridge University Press, Cambridge, 1995).
- [2] E. Ott, *Chaos in Dynamical Systems* (Cambridge University Press, Cambridge, 1993).
- [3] N. van Kampen, *Stochastic processes in physics and chemistry* (North Holland, Amsterdam, 1992).
- [4] C. Gardiner, *Stochastic Methods: A Handbook for the Natural and Social Sciences*, Springer Series in Synergetics (Springer, Berlin, 2009).
- [5] A. Lasota and M. Mackey, *Chaos, fractals, and noise*, 2nd ed., Applied Mathematical Sciences, Vol. 97 (Springer, Berlin, 1994).
- [6] C. Beck and F. Schlögl, *Thermodynamics of Chaotic Systems*, Cambridge nonlinear science series, Vol. 4 (Cambridge University Press, Cambridge, 1993).
- [7] D. Evans and G. Morriss, *Statistical mechanics of nonequilibrium liquids* (Academic Press, London, 1990).
- [8] W. Hoover, *Time reversibility, computer simulation, and chaos* (World Scientific, Singapore, 1999).

- [9] P. Gaspard, *Chaos, scattering, and statistical mechanics* (Cambridge University Press, Cambridge, 1998).
- [10] J. Dorfman, *An introduction to chaos in nonequilibrium statistical mechanics* (Cambridge University Press, Cambridge, 1999).
- [11] R. Klages, *Microscopic chaos, fractals and transport in nonequilibrium statistical mechanics*, Advanced Series in Nonlinear Dynamics, Vol. 24 (World Scientific, Singapore, 2007).
- [12] P. Castiglione, M. Falcioni, A. Lesne, and A. Vulpiani, *Chaos and Coarse Graining in Statistical Mechanics* (Cambridge University Press, Cambridge, 2008).
- [13] F. Reif, *Fundamentals of statistical and thermal physics* (McGraw-Hill, Auckland, 1965).
- [14] L. Reichl, *A Modern Course in Statistical Physics* (Wiley, New York, 2016).
- [15] Y. Kifer, *Ergodic theory of random transformations* (Birkhäuser, Boston, 1986).
- [16] L. Arnold, *Random Dynamical Systems*, Monographs in Mathematics (Springer, Berlin, 1998).
- [17] S. Ulam and J. von Neumann, Bull. Am. Math. Soc. **51**, 660 (1945).
- [18] M. Freidlin, J. Sziucs, and A. Wentzell, *Random Perturbations of Dynamical Systems*, Grundlehren der mathematischen Wissenschaften (Springer, Berlin, 2012).
- [19] C. S. Rodrigues, A. V. Chechkin, A. P. De Moura, C. Grebogi, and R. Klages, Europhys. Lett. **108**, 1 (2014).
- [20] D. Faranda, Y. Sato, B. Saint-Michel, C. Wiertel, V. Padilla, B. Dubrulle, and F. Daviaud, Phys. Rev. Lett. **119**, 014502 (2017).
- [21] M. D. Chekroun, E. Simonnet, and M. Ghil, Physica D **240**, 1685 (2011).
- [22] Y. Sato, T. S. Doan, J. S. W. Lamb, and M. Rasmussen, “Dynamical characterization of stochastic bifurcations in a random logistic map,” (2019), preprint arXiv:1811.03994.
- [23] M. Engel, J. Lamb, and M. Rasmussen, Commun. Math. Phys. **365**, 935 (2019).
- [24] S. Pelikan, Trans. Am. Math. Soc. **281**, 813 (1984).
- [25] A. Lasota and M. C. Mackey, Physica D **28**, 143 (1987).
- [26] M. Blank, Mosc. Math. J. **1**, 315 (2001).
- [27] N. Abbasi, M. Gharaei, and A. J. Homburg, Nonlinearity **31**, 3880 (2018).
- [28] Y. Sato and R. Klages, Phys. Rev. Lett. **122**, 174101 (2019).
- [29] C. Maldonado and R. A. Pérez Otero, Chaos **31** (2021).
- [30] C. Kalle and B. Zeegers, Nonlinearity **36**, 3319 (2023).
- [31] G. Hata and K. Yano, Stochastics and Dynamics **23**, 2350006/1 (2023).
- [32] I. Nisoli, J. Stat. Phys. **190**, 22/1 (2023).
- [33] M. Callaway, T. S. Doan, J. S. W. Lamb, and M. Rasmussen, Annales de l’Institut Henri Poincaré, Probabilités et Statistiques **53**, 1548 (2017).
- [34] M. Engel, J. S. W. Lamb, and M. Rasmussen, Trans. Amer. Math. Soc. **372**, 6343 (2019).
- [35] L. Yu, E. Ott, and Q. Chen, Phys. Rev. Lett. **65**, 2935 (1990).
- [36] E. Van Sebille, M. H. England, and G. Froyland, Env. Res. Lett. **7**, 044040 (2012).
- [37] K. K. Lin and L.-S. Young, Nonlinearity **21**, 899 (2008).
- [38] K. K. Lin, E. Shea-Brown, and L.-S. Young, J. Nonlin. Sci. **19**, 497 (2009).
- [39] A. Pikovsky, Z. Phys. B **55**, 149 (1984).
- [40] H. Fujisaka and T. Yamada, Prog. Theor. Phys. **74**, 918 (1985).
- [41] H. Fujisaka and T. Yamada, Prog. Theor. Phys. **75**, 1087 (1986).
- [42] A. Pikovsky and P. Grassberger, J. Phys. A: Math. Gen. **24**, 4587 (1991).
- [43] N. Platt, E. Spiegel, and C. Tresser, Phys. Rev. Lett. **70**, 279 (1993).
- [44] J. Heagy, N. Platt, and S. Hammel, Phys. Rev. E **94**, 1140 (1994).
- [45] E. Ott and J. Sommer, Phys. Lett. A **188**, 39 (1994).
- [46] H. Hata and S. Miyazaki, Phys. Rev. E **55**, 5311 (1997).
- [47] T. Harada, H. Hata, and H. Fujisaka, J. Phys. A: Math. Gen. **32**, 1557 (1999).
- [48] S. Miyazaki, T. Harada, and A. Budiyo, Prog. Theor. Phys. **106**, 1051 (2001).
- [49] R. Metzler and J. Klafter, Phys. Rep. **339**, 1 (2000).
- [50] R. Klages, G. Radons, and I. M. Sokolov, eds., *Anomalous transport: Foundations and Applications* (Wiley-VCH, Berlin, 2008).
- [51] F. Höfling and T. Franosch, Rep. Prog. Phys. **76**, 046602/1 (2013).
- [52] R. Metzler, J.-H. Jeon, A. G. Cherstvy, and E. Barkai, Phys. Chem. Chem. Phys. **16**, 24128 (2014).
- [53] V. Zaburdaev, S. Denisov, and J. Klafter, Rev. Mod. Phys. **87**, 483 (2015).
- [54] A. Zacherl, T. Geisel, J. Nierwetberg, and G. Radons, Phys. Lett. **114A**, 317 (1986).
- [55] M. Shlesinger, G. Zaslavsky, and J. Klafter, Nature **363**, 31 (1993).
- [56] J. Klafter, M. F. Shlesinger, and G. Zumofen, Phys. Today **49**, 33 (1996).
- [57] G. Zaslavsky, Phys. Rep. **371**, 461 (2002).
- [58] T. Geisel and S. Thomae, Phys. Rev. Lett. **52**, 1936 (1984).
- [59] G. Zumofen and J. Klafter, Phys. Rev. E **47**, 851 (1993).
- [60] R. Artuso and G. Cristadoro, Phys. Rev. Lett. **90**, 244101/1 (2003).
- [61] E. Barkai, Phys. Rev. Lett. **90**, 104101/1 (2003).
- [62] N. Korabel, A. Chechkin, R. Klages, I. Sokolov, and V. Gonchar, Europhys. Lett. **70**, 63 (2005).
- [63] N. Korabel, R. Klages, A. Chechkin, I. Sokolov, and V. Gonchar, Phys. Rev. E **75**, 036213 (2007).
- [64] G. Zaslavsky and D. Usikov, *Weak chaos and quasi-regular patterns*, Cambridge Nonlinear Science Series (Cambridge

University Press, Cambridge, 2001).

- [65] S. Galatolo, *Nonlinearity* **16**, 1219 (2003).
- [66] R. Klages, in *From Hamiltonian Chaos to Complex Systems*, edited by X. Leoncini and M. Leonetti (Springer, Berlin, 2013) pp. 3–42.
- [67] P. Ashwin, P. J. Aston, and M. Nicol, *Physica D* **111**, 81 (1998).
- [68] R. Klages, *Europhys. Lett.* **57**, 796 (2002).
- [69] J. Aaronson, *An introduction to infinite ergodic theory*, Mathematical Surveys and Monographs, Vol. 50 (American Mathematical Society, Providence, 1997).
- [70] R. Zweimüller, “Surrey notes on infinite ergodic theory,” (2009), unpublished.
- [71] E. Aghion, D. A. Kessler, and E. Barkai, *Chaos, Solitons & Fractals* **138**, 109890/1 (2020).
- [72] A. Homburg, C. Kalle, M. Ruziboev, E. Verbitskiy, and B. Zeegers, *Commun. Math. Phys.* **394**, 1 (2022).
- [73] C. Kalle and M. Maggioni, *Erg. Th. Dynam. Sys.* **42**, 141 (2022).
- [74] A. Homburg and C. Kalle, “Iterated function systems of affine expanding and contracting maps on the unit interval,” (2022), preprint arXiv:2207.09987.
- [75] A. Homburg and V. Rabodonandrianandraina, *Erg. Th. Dynam. Sys.* **40**, 1805–1842 (2020).
- [76] Y. Pomeau and P. Manneville, *Commun. Math. Phys.* **74**, 189 (1980).
- [77] P. Manneville, *J. Physique* **41**, 1235 (1980).
- [78] P. Gaspard and X.-J. Wang, *Proc. Nat. Acad. Sci. USA* **85**, 4591 (1988).
- [79] X. Wang, *Phys. Rev. A* **40**, 6647 (1989).
- [80] I. Melbourne and R. Zweimüller, *Annales de l’Institut Henri Poincaré, Probabilités et Statistiques* **51**, 545 (2015).
- [81] M. Thaler, *Israel J. Math.* **46**, 67 (1983).
- [82] M. Thaler, *Israel J. Math.* **37**, 303 (1980).
- [83] R. Zweimüller, *Nonlinearity* **11**, 1263 (1998).
- [84] M. Thaler, *Studia Mathematica* **143**, 103 (2000).
- [85] N. Korabel and E. Barkai, *Phys. Rev. E* **82**, 016209 (2010).
- [86] T. Akimoto and E. Barkai, *Phys. Rev. E* **87**, 032915 (2013).
- [87] T. Chihara, Y. Sato, I. Nisoli, and S. Galatolo, *Chaos*, 032915 (2021).
- [88] T. S. Doan, M. Engel, J. S. Lamb, and M. Rasmussen, *Nonlinearity* **31**, 4567 (2018).
- [89] J. Yan, *Complex Behaviour in Coupled Oscillators, Coupled Map Lattices and Random Dynamical Systems*, Ph.D. thesis, Queen Mary University of London (2021).
- [90] A. Homburg, (2023), private communication.
- [91] C. Beck, *Physica A* **233**, 419 (1996).
- [92] J. Bouchaud, *J. Phys. I* **2**, 1705 (1992).
- [93] G. Bel and E. Barkai, *Phys. Rev. Lett.* **94**, 240602/1 (2005).
- [94] R. Metzler, *Int. J. Mod. Phys. Conf. Ser.* **36**, 1560007 (2015).
- [95] H. Mori, B.-C. So, and T. Ose, *Prog. Theor. Phys.* **66**, 1266 (1981).
- [96] J. Yan and C. Beck, *Chaos, Solitons & Fractals: X* **5**, 100035 (2020).
- [97] L. Fousse, G. Hanrot, V. Lefèvre, P. Pélessier, and P. Zimmermann, *ACM Trans. Math. Softw.* **33**, 13 (2007).
- [98] M. Barnsley, *Fractals everywhere*, 2nd ed. (Academic Press, Boston, 1993).